Ancillary Tethering Influences σ^3-P vs. σ^5-P Speciation and Enables Intermolecular S–H Oxidative Addition to Nontrigonal Phosphorus Compounds

Hye Won Moon,† Ayan Maity,† and Alexander T. Radosevich*

Department of Chemistry, Massachusetts Institute of Technology, Cambridge, Massachusetts 02139, USA

ABSTRACT: The design and synthesis of a nontrigonal phosphorus(III) triamide (**2**) bearing a peripheral ethylene bridge is described. By comparison to a compound lacking the ethylene bridge (**1** (P{N[*o*-NMe-C_6H_4]$_2$}$_3$)), **2** is shown to exclusively form σ^5-P oxidative addition products upon E–H addition (E = OR, SR) in preference to a σ^3-P adduct from cooperative addition across one P–N bond. The resulting pentacoordinate phosphoranes are characterized by multinuclear NMR spectroscopy and X-ray crystallography. DFT calculations on relative energies of σ^3-P and σ^5-P species indicate that the ethylene linker in **2** energetically destabilizes the σ^3-P tautomer of phosphorane product (**2**•[H][E]) by constraining rotation along the C–N bond, favoring formation of σ^5-P phosphoranes by ring-chain tautomerism.

1. INTRODUCTION

Trianionic pincer-type ligands are well-known supporting structures within transition metal organometallic chemistry, [1] and their ability to enforce constrained geometries has likewise found applications in main group chemistry.[2-7] Within this vein, we have reported the preparation of the phosphorus compound **1** based on the trianionic *N*,*N*,*N*-chelate {N[*o*-NMe-C_6H_4]$_2$}$^{3-}$, which adopts a nontrigonal local geometry about phosphorus as a function of the ring constraints (Figure 1, top).[8,9] Whereas the reaction of phosphorus(III) amides with protic pronucleophiles commonly leads to phosphitylation by metathetical exchange,[10,11] compound **1** undergoes intermolecular oxidative addition of amine N–H and alcohol O–H bonds to give pentacoordinate σ^5-P adducts **1**•[H][E] (E= OR, NHR). In situ spectroscopy demonstrated that the observed oxidative addition reactions proceed via a stepwise mechanism involving initial E–H bond cleavage by phosphorus-ligand cooperation,[12] followed by subsequent intramolecular (σ^3-P)→(σ^5-P) tautomerism (Figure 1, top). In the case of volatile amines and alcohols, the reductive elimination from σ^5-P adducts of **1** was also demonstrated, evidently tracing the reverse sequence of steps according to the principle of microscopic reversibility.

As suggested by the reversibility of the oxidative addition, the position of the reversible equilibria depends on the relative stability of the σ^3-P and σ^5-P species. Indeed, in some instances, the overall oxidative addition to **1** is not consummated, but rather the process arrests at the 'open-chain' σ^3-P tautomer. For instance, whereas oxidative addition of methanol proceeds cleanly to the pentacoordinate adduct **1**•[H][OMe], the addition of *tert*-butanol to **1** establishes an equilibrium between σ^3-P and σ^5-P 'ring-chain tautomers' (K_{eq} = 0.51 at 20 °C). Factors governing such ring-chain tautomerism at phosphorus have been discussed by Burgada;[13] it is evident for **1** that steric effects accrue strain to the system that disfavors the σ^5-P oxidative addition product **1**•[H][O^{t}Bu] that is released by tautomerization to the σ^3-P isomer with rotation of one of the C_{aryl}–N bonds.

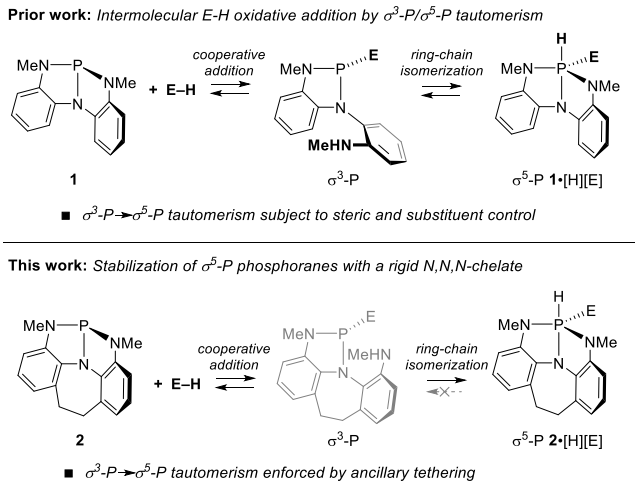

Figure 1. *(top)* Observed equilibrium between hydridophosphoranes and their tautomers upon E–H oxidative addition to nontrigonal phosphorus. *(bottom)* Tethering two aryls with an ethylene linker on the ligand backbone to shift the equilibrium into pentacoordinate phosphoranes from ring-opened tautomers.

In this study, we report the synthesis and reactivity of a geometrically-constrained phosphorus(III) triamide **2**

(P{N[2-NMe-6-CH_2-C_6H_3]$_2$}, Figure 1, bottom) with a designed *N*,*N*,*N*-chelate bearing an ethylene brace on its ligand periphery. This ancillary substitution has negligible effect on the local phosphorus molecular and electronic structure in **2** as compared to **1** and in contrast to a previously reported –CMe_2– linked congener.[7d] Despite the local structurally similarities between **2** and **1**, we find that compound **2** exclusively forms σ^5-phosphoranes upon oxidative addition of O–H bonds of sterically hindered alcohols, phenols, and carboxylic acids. Furthermore, we show that **2** exhibits net intermolecular oxidative addition of S–H bonds, a reaction type not observed for **1** that consequently extends the intermolecular oxidative addition reactivity of nontrigonal phosphorus(III) platforms to a new class of E–H substrates. Together, these results provide evidence of the ability to control conformational and isomer energies by ancillary substituent effects at nontrigonal P(III) in order to steer the course of intermolecular main group oxidative addition reactions.

2. Results and Discussion

2.1 Synthesis and Characterization of 2.

The synthesis of target phosphorus compound **2** was achieved in five steps starting from commercial 10,11-dihydro-5*H*-dibenz[*b*,*f*]azepine (**3,** Scheme 1). The installation of the requisite methylamino moieties present in **2** was initiated by electrophilic bromination of the azepine-based precursor **3** at the 2- and 8-positions with trimethylphenylammonium tribromide. Subsequent electrophilic nitration resulted in isolation of **4**. Heterogeneous catalytic hydrogenation of **4** over carbon-supported palladium in methanol resulted simultaneously in hydrogenolysis of both aryl bromides and reduction of the nitro moieties giving triamine **5**. Two-fold *N*-methylation of **5** by stepwise reductive amination resulted in the *N*,*N*,*N*-chelate **6**, which was treated with PCl_3 and triethylamine[5b-d] to afford the corresponding phosphorus compound **2** in 67% yield as an off-white solid.

Scheme 1. Synthesis of the phosphorus compound 2.

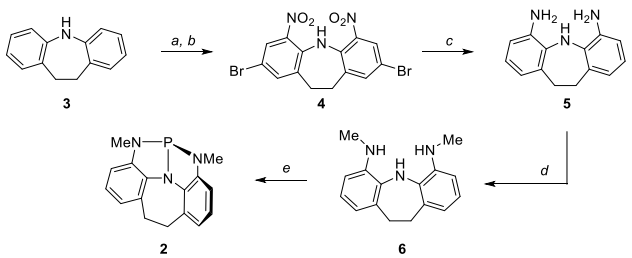

Conditions: (a) $[PhN(CH_3)_3][Br_3]$ (2.0 equiv), MeCN, rt, 4 h, 96%; (b) isoamyl nitrite (3.0 equiv), HNO_3, HOAc, 0 °C, 0.5 h, 84%; (c) Pd/C, H_2 (400 psi), MeOH, rt, 12 h, 66%; (d) paraformaldehyde (10 equiv), NaOMe (4 equiv), MeOH, reflux, 1 h; then, $NaBH_4$, 0 °C → reflux, 1 h, 32%; (d) PCl_3 (1 equiv), NEt_3 (3.5 equiv), THF/Et_2O, 0 °C → rt, 67%.

The $^{31}P\{^1H\}$ NMR spectrum of **2** displayed a resonance at δ 154.2 ppm, which is only modestly upfield from the chemical shift of **1** (159.8 ppm).[5d] In the ^1H NMR spectrum, the six *N*-methyl hydrogens give rise to a single resonance at δ 3.1 ppm which is split into a doublet coupled with phosphorus ($^3J_{P-H}$ = 8.1 Hz). The four protons in the ethylene backbone are also magnetically equivalent as a single resonance observed at δ 3.2 ppm. The six aryl hydrogens give rise to three resonances, indicating a time-averaged molecular geometry of C_s symmetry at ambient temperature.

A crystalline sample of **2** suitable for X-ray diffraction was grown by vapor diffusion of pentane into a tetrahydrofuran solution. Overall, compound **2** adopts a molecular structure of C_1 symmetry in its solid state as a function of the puckering enforced by ethylene bridge (Figure 2), but local geometrical parameters for **2** are remarkably similar to those for **1**. Folding along the P_1–N_1 axis gives a bond angle between the phosphorus and the two remote nitrogens ∠N_2–P_1–N_3 = 115.67(8)° for **2**, nearly identical to that found for **1** (∠N_2–P_1–N_3 = 115.21(7)°) (cf. Table 1). Also, the two interior angles between phosphorus and two proximal nitrogen atoms are nearly equivalent (∠N_1–P_1–N_2 = 89.59(6)° and ∠N_1–P_1–N_3 = 89.98(9)°) as those of **1** (90.51(6)° and ∠N_1–P–N_3 = 90.08(6)°).

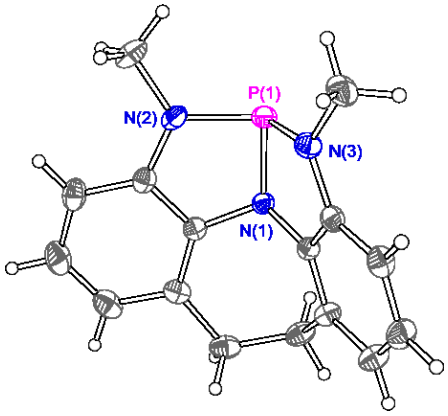

Figure 2. Thermal ellipsoid plot of **2** rendered at 50% probability level. Selected bond distances (Å) and angles (◦): *d*(P_1–N_1) = 1.7592(9); *d*(P_1–N_2) = 1.7009(10); *d*(P_1–N_3) = 1.7259(10); ∠N_1–P_1–N_2 = 89.60(5); ∠N_1–P_1–N_3 = 89.99(4); ∠N_2–P_1–N_3 = 115.68(5).

Table 1. Tabulated bond distances (Å), angles (°), and δ (ppm) values for selected compounds.[a]

Metric	**1**[b]	**2**	**2**•[H][SBn]
d(P_1–N_1)	1.7610(12)	1.7592(9)	1.7830(11)
d(P_1–N_2)	1.7014(14)	1.7009(10)	1.7021(13)
d(P_1–N_3)	1.7190(13)	1.7259(10)	1.7088(13)
d(P_1–H_1)	—	—	1.36(2)
d(P_1–S_1)	—	—	2.1369(5)
∠N_1–P_1–H_1	—	—	173.7(10)
∠N_1–P_1–S_1	—	—	92.69(4)
∠N_1–P_1–N_2	90.51(6)	89.60(5)	86.57(6)
∠N_1–P_1–N_3	90.08(6)	89.99(4)	87.70(6)
∠N_2–P_1–N_3	115.21(7)	115.68(5)	135.32(6)
δ ^{31}P	159.8	154.2	–23.8

[a] See SI for full details. [b] Data from Ref. 5d.

Although the C_1 symmetry of the solid state renders all four hydrogen nuclei in the ethylene linker diastereotopic in principle, these four ethylene protons resonate as a sin-

glet at δ 3.1 ppm in ^{1}H NMR spectrum (toluene-d_8, 25 °C). By contrast, two partially resolved doublets (Δν = 30 Hz) are observed at −80 °C, with an estimated coalescence temperature (T_c) of ca. −75 °C (Figure 3, top). The rate constant for this dynamic process was calculated by simulating the ^{1}H NMR that were collected over the temperature range of −10 °C > T > −90 °C. A line shape analysis and the resulting Eyring plot indicate the free energy of activation for the dynamic process to be $\Delta G^{\ddagger}_{exptl}{}^{298}$ = 8.7 kcal/mol (see the Supporting Information for full details). The small activation entropy for the interconversion process ($\Delta S^{\ddagger}_{exptl}$ = 2.2 cal/mol•K) also supports the unimolecular process. Over the entire temperature range (25 °C > T > −90 °C), the ^{31}P chemical shift of **2** remains unchanged (δ 154.2 ppm). By analogy to related conformational isomerism of **1**,[5d] we assign the structural dynamics of **2** to an edge-inversion at phosphorus[14] that interconverts the ethylene C–H positions on the concave and convex faces of the equilibrium structure of **2** (Figure 3, bottom). The observed peak separation and T_c indicate that the ethylene linker has a negligible effect on the edge-inversion process which has been observed with the compound **1** analogue ($\Delta G^{\ddagger}_{exptl}{}^{298}$ = 10.7(5) kcal/mol).[5d] The low barrier to inversion is distinguished from typical vertex inversion barriers at tricoordinate phosphorus ($\Delta G^{\ddagger}$ ≈ 30-35 kcal/mol)[15] but conforms to observations in other phosphabicyclic systems.[5e,14]

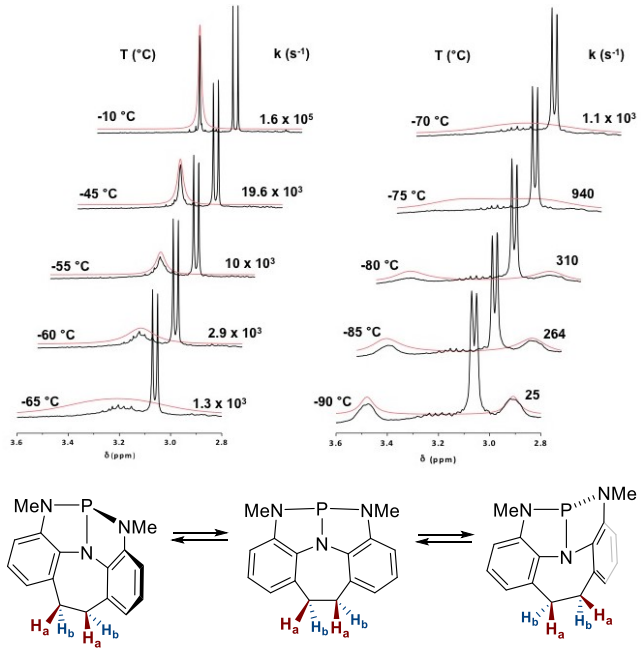

Figure 3. *(top)* Variable temperature ^{1}H NMR spectra of **2** showing the decoalescence of the diastereotopic protons in the ethylene linker below −75 °C. Experimental spectra in black, simulated spectra in red. See the SI for fitting parameters and Eyring analysis. *(bottom)* An edge-inversion process at phosphorus of **2** and the resulting chemical exchange between protons on the concave and the convex side.

To examine the impact of the ethylene linker on the electronic character of **2**, we analyzed the $^1J_{31P-77Se}$ coupling constant for the terminal selenide **2**•[Se] readily formed by treatment with elemental selenium. The magnitude of the coupling constant (J = 906 Hz) suggests high *s*-character in the lone pair at phosphorus, comparable to that for **1**•[Se] (J = 907 Hz) but significantly greater than for $(Me_2N)_3P$ (J = 784 Hz).[16] Natural bond orbital (NBO) analysis[17] of a DFT (B3LYP/Def2-TZVP) model of **2** implies a phosphorus-based lone pair with $sp^{0.60}$ hybridization (62.3% s-orbital character), in line with that observed for **1** ($sp^{0.62}$ hybridization, 61.7% s-orbital character). Similarly, the calculated frontier orbital energies of **1** and **2** show marginal difference in electronic structure between **1** and **2,** with nearly identical frontier orbital energies (E_{HOMO} = −5.13 eV, E_{LUMO} = −0.58 eV for **1** and E_{HOMO} = −5.07 eV, E_{LUMO} = −0.62 eV for **2**) and an orbital gap of ca. 4.5 eV (see Supporting Information for full details).

In sum, our results indicate that the inclusion of the ethylene linker of **2** has no significant impact on ground state geometry, dynamic structure, or lone pair electronic character of the nontrigonal phosphorus compound as compared to the nontethered congener **1.**

2.2 O–H Addition Reactivity of 2.

To evaluate the impact of the peripheral ethylene linker in **2** on the σ^3-P/σ^5-P speciation in E–H oxidative addition, we examined the reactivity of **2** toward tertiary alcohols. Treatment of compound **2** (^{31}P NMR δ 154.2 ppm) with *tert*-butyl alcohol in chloroform-*d* resulted in quantitative formation of σ^5-P *tert*-butoxy hydrido phosphorane **2**•[H][O^{t}Bu] (^{31}P NMR δ −37.6 ppm, $^1J_{P-H}$ = 598 Hz, $^3J_{P-H}$ = 17 Hz), without detection of its σ^3-P tautomer **8**•[O^{t}Bu] (Figure 4). This spectroscopic data is in line with the analogous compound **1**•[H][O^{t}Bu] (^{31}P NMR δ −37.5 ppm, $^1J_{P-H}$ = 578 Hz, $^3J_{P-H}$ = 17.4 Hz).[5d] The protons of the ethylene bridge in **2**•[H][O^{t}Bu] give rise to two multiplet peaks in the ^{1}H NMR spectrum (δ 3.37 – 3.30 (m, 2H), 3.13 – 3.04 (m, 2H) ppm) corresponding to *syn* and *anti* pairs with respect to the addend *tert*-butoxy group.

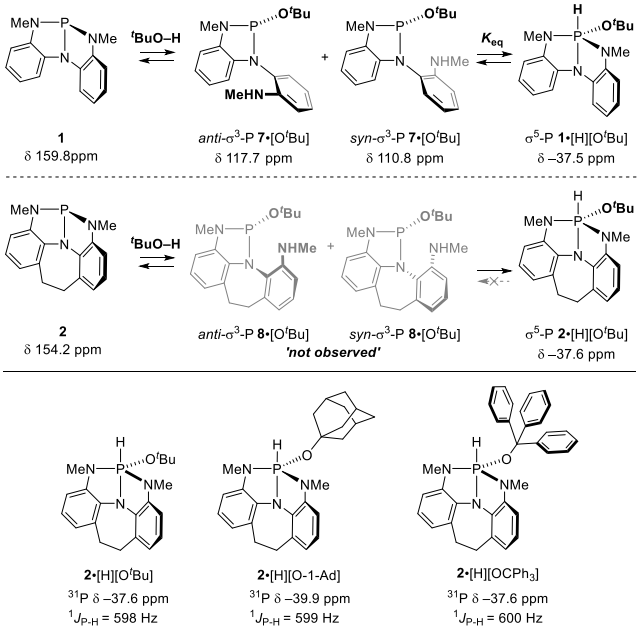

Figure 4. Oxidative addition of O–H bond in tertiary alcohols to **1** and **2**, and examples of stable hydridoalkoxyphosphoranes including key ^{31}P NMR parameters.

In similar fashion, the addition of 1-adamantanol (1-AdOH) and triphenylmethanol (Ph_3COH) to **2** were also shown to form σ^5-P oxidative addition products exclusively (^{31}P NMR δ −39.9 (**2**•[H][O-1-Ad]) and δ −37.6 ppm

(**2**•[H][$OCPh_3$])). Importantly, addition of these same bulky tertiary alcohols to compound **1** does not lead to clean formation of the corresponding σ^5-P oxidative addition products; instead, an equilibrium mixture of σ^3-P/σ^5-P ring-chain tautomers is observed (Figure S4 and S5). It is evident that the presence of the remote ethylene bridge has a marked impact on the speciation of the addition reaction between **2** and sterically encumbered alcohols.

In addition to controlling the thermodynamic position of the ring-chain tautomer equilibrium, evidence suggests that the ethylene bridge in **2** also leads to enhanced kinetic reactivity of this nontrigonal phosphorus(III) triamide in E–H oxidative addition. Specifically, when monitored by ^{31}P NMR spectroscopy, the reaction of **2** and *p*-methoxyphenol was found to proceed completely to phosphorane adduct **2**•[H][OC_6H_4OMe] within 10 min and without the observation of any σ^3-P intermediates **8**•[OC_6H_4OMe]. For reference, the analogous reaction of *p*-methoxyphenol with compound **1** requires more than 16 h to proceed to completion via long-lived σ^3-P intermediates. A related phenomenon is found for O–H oxidative addition of carboxylic acids. Again, the oxidative addition of *p*-toluic acid to **2** was complete in 10 min to give **2**•[H][O_2C-C_6H_4Me] without detectable σ^3-P intermediates **8**•[O_2C-C_6H_4Me], whereas the corresponding addition reaction with compound **1** required 48 h for completion via observable σ^3-P intermediates (Figure S7).

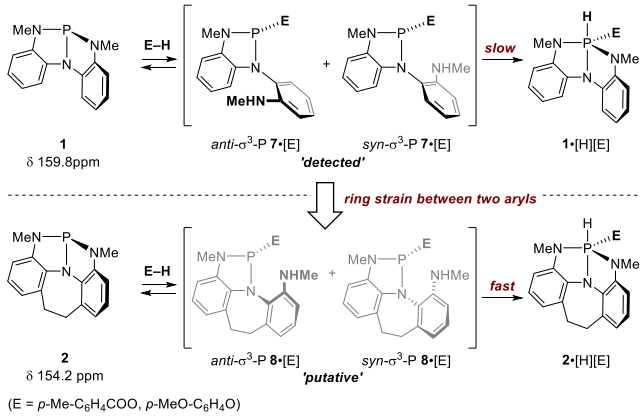

Figure 5. Effects of the ethylene linker in **2** on the reaction intermediates and kinetics in E–H oxidative addition to phosphorus(III) triamide.

2.3 S–H Addition Reactivity of 2.

The addition of thiols to nontrigonal phosphorus(III) triamides has not been previously reported, but comparative study of **1** and **2** in S–H oxidative addition provides evidence for the importance of the peripheral ethylene bridge of **2** in controlling reaction outcome. The addition of benzyl mercaptan to compound **1** was monitored by ^{31}P NMR spectroscopy in toluene-d_8 at ambient temperature. The signal for **1** (δ 159.8 ppm) was consumed over the course of 24 h and replaced by two singlets at δ 156.4 and δ 149.3 ppm, which were assigned to the two atropisomeric σ^3-P compounds *syn*-**7**•[SBn] and *anti*-**7**•[SBn] (Figure 6, top). No further conversion of *syn*-**7**•[SBn] and *anti*-**7**•[SBn] into σ^5-P tautomer **1**•[H][SBn] was observed over the ensuing two weeks, indicating that **1** cannot form stable σ^5-P thiol adducts due to the stable σ^3-P isomers.

By contrast, a parallel experiment monitoring the addition of benzyl mercaptan to **2** shows within 48 h the clean formation of a single new peak in the pentacoordinate region of ^{31}P{^{1}H} NMR chemical shift range at δ –32.5 ppm. In the proton coupled ^{31}P NMR spectrum, the peak at δ –32.5 ppm appears as a doublet of triplets of heptets ($^1J_{P–H}$ = 564 Hz, $^3J_{P–H}$ = 20, 18 Hz) marked by a large $^1J_{P–H}$ coupling constant indicative of a direct P–H bond. Complementary couplings were discerned in the ^{1}H NMR spectrum at δ 6.7 ppm for phosphorus-bound hydrogen as a broad doublet, at δ 3.4 ppm for two benzylic hydrogen as a doublet, and at δ 2.6 ppm for N-methyl groups as a doublet. The combined multinuclear spectral data are consistent with the formation of a σ^5-P phosphorane **2**•[H][SBn].

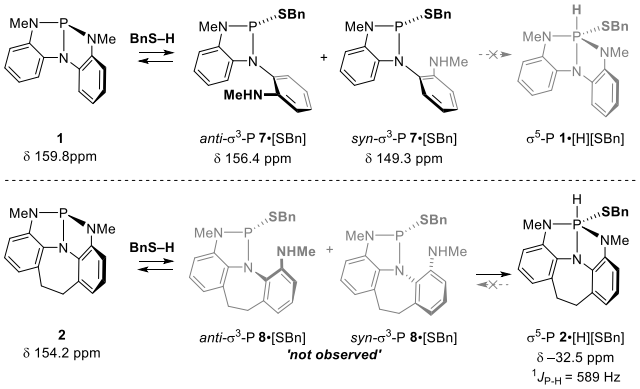

Figure 6. Different reactivity of compound **1** and **2** toward benzyl mercaptan.

To corroborate the S–H oxidative addition, crystalline solids of **2**•[H][SBn] were grown by vapor diffusion from a toluene/pentane system. X-ray diffraction confirms the trigonal bipyramidal structure of the *N*,*N*,*N*-chelated pentacoordinate phosphorane **2**•[H][SBn], with an apical hydrido- and an equatorial benzylthio- substituent (Figure 7). The observation that **2**•[H][SBn] possesses an apical hydride falls in line with prior observations regarding the relative positional display of substituents upon E–H oxidative addition to nontrigonal σ^3-P. Indeed, given that the thio group has similar apicophilicity to an alkoxy group,[18] the observed structure indicates that the ethylene linker on the ligand backbone does not subvert the negative hyperconjugation that has been proposed to stabilize apical hydrides following E–H oxidative addition.[5d]

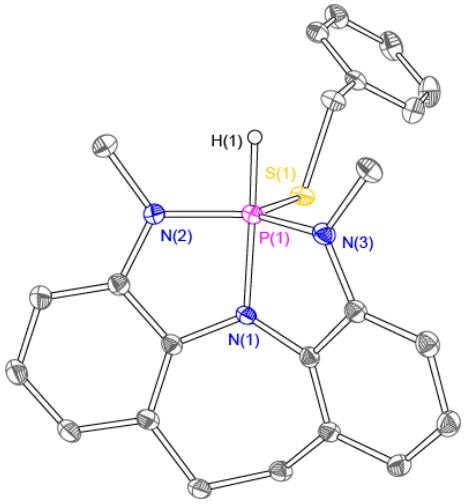

Figure 7. Thermal ellipsoid plot of **2**•[H][SBn] rendered at 50% probability level with all carbon-based hydrogen atoms omitted for clarity. Selected bond distances (Å) and angles (◦): $d(P_1–N_1)$ = 1.7830(11); $d(P_1–N_2)$ = 1.7021(13); $d(P_1–N_3)$ = 1.7088(13); $d(P_1–H_1)$ = 1.36(2); $d(P_1–S_1)$ = 2.1369(5); $\angle N_1–P_1–N_2$ = 86.57(6); $\angle N_1–P_1–N_3$ = 87.70(6); $\angle N_2–P_1–N_3$ = 135.32(6); $\angle N_1–P_1–H_1$ = 173.7(10); $\angle N_1–P_1–S_1$ = 92.69(4). τ = 0.64 ($\angle H_1–P_1–N_1 – \angle N_2–P_1–N_3$)/60).

To rationalize the observed differences between **1** and **2** in S–H oxidative addition, the reaction thermochemistry for the addition of MeS–H was calculated at the ωB97X-D3/6-311++G(2d,2p) level of theory. Although O–H oxidative addition to **1** is significantly downhill (ΔG ≈ –10 kcal/mol), the formation of **1**•[H][SMe] from **1** and MeS–H is computed to have a much smaller driving force (ΔG_{calc} = –0.3 kcal/mol) (Figure 8, top). Interestingly, the S–H oxidative addition of MeS–H to **2** is calculated similarly to be nearly thermoneutral (ΔG_{calc} = –0.7 kcal/mol, respectively). It is concluded that the difference in observed S–H oxidative addition outcomes cannot be attributed to a driving force difference. Instead, a consideration of the relative stabilities of the σ³-P isomers is apt. For the addition to **1**, the σ³-P tautomer **7**•[SMe] is more stable than σ⁵-P **1**•[H][SMe] by 6.6 kcal/mol. By contrast, for the addition to **2**, the σ³-P tautomer **8**•[SMe] is more unstable than σ⁵-P **1**•[H][SMe] by 8.6 kcal/mol. In effect, the ethylene linker on the ligand backbone of **2** prevents rotation of the C_{aryl}–N bond in σ³-P tautomer **8**•[SMe] ($\angle P_1–N_1–C–C$ = 95.3° in **7**•[SMe] vs. $\angle P_1–N_1–C–C$ = 38.9◦ in **8**•[SMe]) resulting in a shift of the equilibrium from the σ³-P tautomer **8**•[SMe] to σ⁵-P **2**•[H][SMe]. Both enthalpic (ΔH_{calc} = –9.6 kcal/mol for σ³-P **8**• [SMe] → σ⁵-P **2**•[H][SMe], vs. ΔH_{calc} = +4.5 kcal/mol for σ³-P **7**•[SMe] → σ⁵-P **1**•[H][SMe]) and entropic (ΔS_{calc} = –3.4 cal/mol•K for σ³-P **8**•[SMe] → σ⁵-P **2**•[H][SMe], vs. ΔS_{calc} = –6.7 cal/mol•K for σ³-P **7**•[SMe] → σ⁵-P **1**•[H][SMe]) contributions reinforce the preferential formation of **2**•[H][SMe] over **8**•[SMe], as compared to **1**•[H][SMe]/**7**•[SMe].

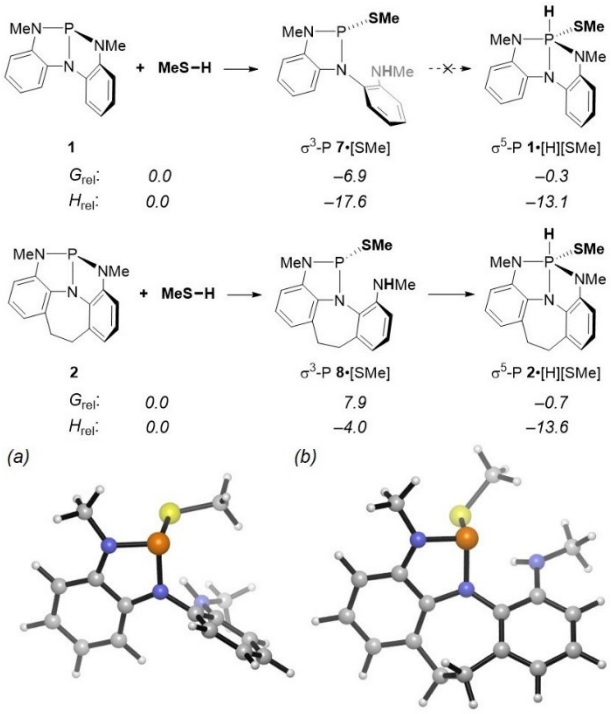

Figure 8. Computational results (ωB97X-D3/6-311++G(2d,2p)) for S–H oxidative addition by **1** and **2**. *(top)* Computed relative free energies and enthalpies in kcal/mol; *(bottom)* DFT models of (a) **7**•[SMe], σ³-P tautomer of **1**•[H][SMe] and (b) **8**•[SMe], σ³-P tautomer of **2**•[H][SMe].

3. Conclusion

The *N,N,N*-chelating pocket of triamine **6** bearing an ancillary ethylene tether between two aryl groups readily accommodates phosphorus in both the tri- and pentacoordinate states. As compared to compound **1** lacking the remote ethylene linker, the presence of the ancillary substitution results in little to no change in local structure and bonding in the σ³-P compound **2**. However, compound **2** facilitates the intermolecular E–H oxidative addition at phosphorus, both thermodynamically and kinetically, by constraining C_{aryl}–N bond rotation of the tricoordinate tautomers and thereby enforcing access to pentacoordination upon E–H bond cleavage processes. Investigations of compound **2** to explore new E–H cleavage reactivity through control of relative σ³-P/σ⁵-P energies by ancillary tethering are ongoing.

4. Experimental Section

Full experimental details are available in the online supplementary information.

4.1 General procedure for O–H oxidative addition. To a solution of phosphorus(III) compound **2** (14 mg, 0.05 mmol, 1 equiv) in dry chloroform-*d* (0.5 mL) was added a solution of ROH (0.05 mmol, 1 equiv) in dry chloroform-*d* (0.5 mL). The solution was monitored by ^{31}P NMR spectroscopy until complete conversion to corresponding phosphorus(V) species was observed (typically within 15 min).

4.2 Procedure for S–H oxidative addition. A solution of **2** (14 mg, 0.05 mmol) and benzyl mercaptan (12 μL, 2

equiv, 0.1 mmol) in toluene-d_8 (0.5 mL) was stirred at ambient temperature for 48 h. The volatiles ware removed in vacuo. The resulting solid was washed with pentane three times and dried under vacuum to afford the pentacoordinate product. ^{1}H NMR (400 MHz, toluene-d_8) δ 7.06 – 6.90 (m, 5H), 6.86 (t, J = 7.7 Hz, 2H), 6.67 (d, $^1J_{P-H}$ = 563.5 Hz, 1H), 6.62 (d, J = 7.8 Hz, 2H), 6.42 (d, J = 7.6 Hz, 2H), 3.41 (d, $^3J_{P-H}$ = 20.0 Hz, 2H), 3.11 – 3.02 (m, 2H), 2.85 – 2.75 (m, 2H), 2.56 (d, $^3J_{P-H}$ = 18.4 Hz, 6H) ppm. ^{13}C NMR (101 MHz, toluene-d_8) δ 139.95 (d, $^3J_{P-C}$ = 4.0 Hz), 132.69 (d, $^2J_{P-C}$ = 12.3 Hz), 130.91 (d, $^2J_{P-C}$ = 15.1 Hz), 128.80, 128.39, 126.70, 125.54 (d, $^3J_{P-C}$ = 9.7 Hz), 121.40 (d, $^4J_{P-C}$ = 1.9 Hz), 120.69, 107.58 (d, $^3J_{P-C}$ = 7.3 Hz), 34.56, 32.98, 27.76 (d, $^2J_{P-C}$ = 15.9 Hz) ppm. ^{31}P{^{1}H} NMR (toluene-d_8, 162 MHz): –32.45 ppm. ^{31}P NMR (toluene-d_8, 162 MHz): –32.45 (dthept, J = 563.5, 20.0, 18.4 Hz) ppm. HRMS (DART) calculated for $C_{23}H_{25}N_3PS$ (M+H) 406.1501 found 406.1495.

4.3 Variable temperature NMR spectra of 2. In an inert atmosphere glovebox, compound **2** (7 mg, 0.025 mmol) was dissolved in toluene-d_8 (1 mL). The sample was then transferred to a sealable J-Young NMR tube. Variable temperature NMR experiments were recorded on a Bruker AVANCE-400 spectrometer. ^{1}H and ^{31}P NMR spectra were recorded at temperature intervals between –10 °C > T > –90 °C. The sample and probe were thermostatted at each temperature for 5 min before spectra were recorded. At the end of the experiment, a spectrum at room temperature was recorded to verify the reversibility of the temperature dependent process. Line-shape fitting was performed using the WinDNMR software package.[19] All chemical shifts, coupling constants, and line width values were set based on values derived from the experimental spectra. The exchange rate variable was adjusted to fit the overlaid experimental spectrum at each temperature.

4.4 X-ray diffraction Methods. Diffraction data for compound **2** and **2•**[H][SBn] were collected on a Bruker-AXS X8 Kappa Duo diffractometer coupled to a SMART Apex II CCD detector with Mo K_α radiation (λ = 0.71073 Å) from an IμS micro-source, performing φ-and ω-scans at 100 K. Crystals were mounted on a glass fiber pin using Paratone N oil. The SMART program package was used for determination of the unit-cell parameters and for data collection. The raw frame data were processed using SAINT[20] and SADABS[21] to yield the reflection data file. The structures were solved by direct methods using SHELXT[22] and refined against F^2 on all data by full-matrix least squares with SHELXL-2016[23] following established refinement strategies.[24] All non-hydrogen atoms were refined anisotropically, and all hydrogen atoms were included into the model at geometrically calculated positions and refined using a riding model. The isotropic displacement parameters of all hydrogen atoms were fixed to 1.2 times the U value of the atoms they are linked to. Details of the data quality and a summary of the residual values of the refinements are listed in Supporting Information.

4.5 Computational Methods. Geometries were optimized in ORCA using the ωB97X-D3 density functional with the 6-311+ +G(2d,2p) basis set. Methanethiol was used as a model thiol; the complete compound **2** was modelled. See Supporting Information for further details.

ASSOCIATED CONTENT

Supporting Information

The Supporting Information is available free of charge on the ACS Publications website.
Full experimental procedures; ^{1}H, ^{13}C and ^{31}P NMR spectra; crystallographic details; computational details (.pdf)
Crystallographic files (.cif)
Cartesian coordinates (.xyz)

AUTHOR INFORMATION

Corresponding Author

* radosevich@mit.edu

Notes

† These authors contributed equally.

The authors declare no competing financial interests.

ACKNOWLEDGMENT

We gratefully acknowledge funding support from NSF (CHE-1900060) and MIT. We thank Jared Mattos for preliminary synthetic work and Dr. Peter Mueller (MIT) for assistance with crystallographic data collection.

REFERENCES

[1] For a review of trianionic pincer complexes: O'Reilly, M. E.; Veige, A. S., Trianionic pincer and pincer-type metal complexes and catalysts. *Chem. Soc. Rev.* **2014**, *43*, 632.

[2] B compounds: (a)Huang, K.; Dutton, J. L.; Martin, C. D. Exploiting Pincer Ligands to Perturb the Geometry at Boron. *Chem. Euro. J.* **2017**, *23*, 10532-10535. (b) Janes, T.; Diskin-Posner, Y.; Milstein, D. Synthesis and Reactivity of Cationic Boron Complexes Distorted by Pyridine-based Pincer Ligands: Isolation of a Photochemical Hofmann–Martius-type Intermediate. *Angew. Chem. Int. Ed.* **2020**, *59*, 4932-4936.

[3] Al compounds: (a) Koller, J.; Bergman, R. G. Synthesis, Characterization, and Reactivity of Aluminum Alkyl/Amide Complexes Supported by Guanidinate and Monoanionic OCO-Pincer Ligands. *Organometallics* **2010**, *29*, 3350-3356. (b) Myers, T. W.; Berben, L. A. Aluminum–Ligand Cooperative N–H Bond Activation and an Example of Dehydrogenative Coupling. *J. Am. Chem. Soc.* **2013**, *135*, 9988-9990. (c) Myers, T. W.; Berben, L. A. Aluminum–Amido-Mediated Heterolytic Addition of Water Affords an Alumoxane. *Organometallics* **2013**, *32*, 6647-6649.

[4] Si compounds: Kramer, N.; Jöst, C.; Mackenroth, A.; Greb, L. Synthesis of Electron-Rich, Planarized Silicon(IV) Species and a Theoretical Analysis of Dimerizing Aminosilanes. *Chem. Euro. J.* **2017**, *23*, 17764-17774.

[5] P compounds: (a) Arduengo, A. J.; Stewart, C. A.; Davidson, F.; Dixon, D. A.; Becker, J. Y.; Culley, S. A.; Mizen, M. B. The Synthesis, Structure, and Chemistry of 10-Pn-3 Systems: Tricoordinate Hypervalent Pnicogen Compounds. *J. Am. Chem. Soc.* **1987**, *109*, 627-647. (b) Dunn, N. L.; Ha, M. J.; Radosevich, A. T. Main Group Redox Catalysis: Reversible P-III/P-V Redox Cycling at a Phosphorus Platform. *J. Am. Chem. Soc.* **2012**, *134*, 11330-11333. (c) McCarthy, S. M.; Lin, Y.-C.; Devarajan, D.; Chang, J. W.; Yennawar, H. P.; Rioux, R. M.; Ess, D. H.; Radosevich, A. T. Intermolecular N–H Oxidative Addition of Ammonia, Alkylamines, and Arylamines to a Planar σ3-Phosphorus Compound via an Entropy-Controlled Electrophilic Mechanism. *J. Am. Chem. Soc.* **2014**, *136*, 4640-4650. (d) Zhao, W.; McCarthy, S. M.; Lai, T. Y.; Yennawar, H. P.; Radosevich, A. T. Reversible Intermolecular E–H Oxidative Addition to a Geometrically Deformed and Structurally Dynamic Phosphorous Triamide. *J. Am. Chem. Soc.* **2014**, *136*, 17634-17644. (e) Robinson, T. P.; De Rosa, D. M.; Aldridge, S.; Goicoechea, J. M. E–H Bond Activation of Ammonia and Water by

a Geometrically Constrained Phosphorus(III) Compound. *Angew. Chem. Int. Ed.* **2015**, *54*, 13758-13763.

[6] Bi compounds: (a) Wang, F.; Planas, O.; Cornella, J. Bi(I)-Catalyzed Transfer-Hydrogenation with Ammonia-Borane. *J. Am. Chem. Soc.* **2019**, *141*, 4235-4240. (b) Kindervater, M. B.; Marczenko, K. M.; Werner-Zwanziger, U.; Chitnis, S. S. A Redox-Confused Bismuth(I/III) Triamide with a T-Shaped Planar Ground State. *Angew. Chem. Int. Ed.* **2019**, *58*, 7850-7855. (c) Marczenko, K. M.; Jee, S.; Chitnis, S. S. High Lewis Acidity at Planar, Trivalent, and Neutral Bismuth Centers. *Organometallics* **2020**, DOI: 10.1021/acs.organomet.0c00378.

[7] (a) Pistner, A. J.; Moon, H. W.; Silakov, A.; Yennawar, H. P.; Radosevich, A. T. Stable Open-Shell Phosphorane Based on a Redox-Active Amidodiphenoxide Scaffold. *Inorg. Chem.* **2017**, *56*, 8661-8668. (b) Sherbow, T. J.; Fettinger, J. C.; Berben, L. A. Control of Ligand pKa Values Tunes the Electrocatalytic Dihydrogen Evolution Mechanism in a Redox-Active Aluminum(III) Complex. *Inorg. Chem.* **2017**, *56*, 8651-8660. (c) Robinson, T. P.; De Rosa, D.; Aldridge, S.; Goicoechea, J. M. On the Redox Reactivity of a Geometrically Constrained Phosphorus(III) Compound. *Chem. Euro. J.* **2017**, *23*, 15455-15465. (d) Mondal, M. K.; Zhang, L.; Feng, Z.; Tang, S.; Feng, R.; Zhao, Y.; Tan, G.; Ruan, H.; Wang, X. Tricoordinate Nontrigonal Pnictogen-Centered Radical Anions: Isolation, Characterization, and Reactivity. *Angew. Chem. Int. Ed.* **2019**, *58*, 15829-15833.

[8] Abbenseth, J.; Goicoechea, J. M., Recent developments in the chemistry of non-trigonal pnictogen pincer compounds: from bonding to catalysis. *Chem. Sci.* **2020,** *11,* 9728-9740.

[9] (a) Tanushi, A.; Radosevich, A. T. Insertion of a Nontrigonal Phosphorus Ligand into a Transition Metal-Hydride: Direct Access to a Metallohydrophosphorane. *J. Am. Chem. Soc.* **2018**, *140*, 8114-8118. (b) Lee, K.; Blake, A. V.; Tanushi, A.; McCarthy, S. M.; Kim, D.; Loria, S. M.; Donahue, C. M.; Spielvogel, K. D.; Keith, J. M.; Daly, S. R.; Radosevich, A. T. Validating the Biphilic Hypothesis of Nontrigonal Phosphorus(III) Compounds. *Angew. Chem. Int. Ed.* **2019**, *58*, 6993-6998. (c) Cleveland, G. T.; Radosevich, A. T. A Nontrigonal Tricoordinate Phosphorus Ligand Exhibiting Reversible "Nonspectator" L/X-Switching. *Angew. Chem. Int. Ed.* **2019**, *58*, 15005-15009.

[10] Nifantiev, E. E.; Grachev, M. K.; Burmistrov, S. Y., Amides of Trivalent Phosphorus Acids as Phosphorylating Reagents for Proton-Donating Nucleophiles. *Chem. Rev.* **2000,** *100*, 3755-3800.

[11] For applications in modern oligonucleotide synthesis: (a) Beaucage, S. L.; Caruthers, M. H. Deoxynucleosidephosphoramidites–a new class of key intermediates for deoxypolynucleotide synthesis. *Tetrahedron Lett.* **1981**, *22*, 1859–1862. (b) Caruthers, M. H. Gene synthesis machines: DNA chemistry and its uses. Science 1985, 230, 281-285. (c) Reese, C. B. Oligo- and polynucleotides: 50 years of chemical synthesis. *Org. Biomol. Chem.* **2005**, *3*, 3851-3868.

[12] Greb, L.; Ebner, F.; Ginzburg, Y.; Sigmund, L. M., Element-Ligand Cooperativity with p-Block Elements. *Eur. J. Inorg. Chem.* **2020,** 3030-3047.

[13] (a) Burgada, R.; Setton, R. "Preparation, Properties and Reactions of Phosphoranes." In *The Chemistry of Organophosphorus Compounds*; Hartley, F., Ed.; Wiley: Chichester, **1994**; Vol. 3, pp 185. (b) Bernard, D.; Laurenco, C.; Burgada, R., Mécanisme de formation et de transformation des spirophosphoranes: III. Synthèse et tautomérie PIII⇌PV des tétraoxyspirophosphoranes á liaison P–H. *J. Organomet. Chem.* **1973,** *47*, 113-123. (c) Burgada, R.; Laurenço, C., Mécanisme de formation et de transformation des spirophosphoranes: V. Synthèse et tautomérie PIII ⇌ PV des spirophosphoranes liaison P–H dérivant des α aminoalcools substitués au carbone et à l'azote. *J. Organomet. Chem.* **1974,** *66*, 255-270. (d) Burgada, R. Spirophosphoranes. Synthèses, structure, and réactivité. *Bull. Soc. Chim. Fr.* **1975**, 407-424. (e) Muñoz, A. Application de la théorie de Pearson aux composés organophosphorés. Spirophosphoranes à liaison P-H-Tautomérie. *Bull. Soc. Chim. Fr.* **1977**, 728-736.

[14] Arduengo, A. J.; Dixon, D. A.; Roe, D. C. Direct determination of the barrier to edge inversion at trivalent phosphorus: verification of the edge inversion mechanism. *J. Am. Chem. Soc.* **1986**, *108*, 6821-6823.

[15] (a) Baechler, R. D.; Mislow, K. Effect of structure on the rate of pyramidal inversion of acyclic phosphines. *J. Am. Chem. Soc.* **1970**, *92*, 3090-3093. (b) Marynick, D. S.; Dixon, D. A. Electronic structure of phosphine. Effect of basic set and correlation on the inversion barrier. *J. Phys. Chem.* **1982,** *86*, 914-917. (c) Mukhlall, J. A.; Hersh, W. H. Measurement of the barrier to inversion of configuration in acyclic phosphite triesters. *Inorg. Chim. Acta* **2011**, *369*, 62-70.

[16] Allen, D. W.; Taylor, B. F. The chemistry of heteroarylphosphorus compounds. Part 15. Phosphorus-31 nuclear magnetic resonance studies of the donor properties of heteroarylphosphines towards selenium and platinum(II). *J. Chem. Soc. Dalton Trans.* **1982**, 51-54.

[17] NBO 6.0: Glendening, E. D., Badenhoop, J. K., Reed, A. E., Carpenter, J. E., Bohmann, J. A., Morales, C. M., Landis, C. R., and Weinhold, F., Theoretical Chemistry Institute, University of Wisconsin, Madison, WI, 2013.

[18] Bone, S.; Trippett, S.; Whittle, P. J. The apicophilicity of thio-substituents in trigonal bipyramidal phosphoranes. *J. Chem. Soc., Perkin Trans. 1* **1974**, 2125-2132.

[19] Reich, H. J. *J. Chem. Educ. Software* **1996**, *3D*, 2.

[20] SAINT; Bruker AXS, Inc.: Madison, WI, 2013.

[21] Sheldrick, G. M. SADABS; Bruker AXS, Inc.: Madison, WI, 2014.

[22] Sheldrick, G. M. *Acta Crystallogr. SHELXT* – Integrated space-group and crystal-structure determination. **2015**, *A71*, 3.

[23] Sheldrick, G. M., *Acta Crystallogr.* Crystal structure refinement with *SHELXL*. **2015**, *C71*, 3.

[24] Müller, P. Practical suggestions for better crystal structures. *Cryst. Rev.* **2009**, *15*, 57.

TOC Graphic